

Coincident excitation and radiative decay in electron-nucleus collisions

D. H. Jakubassa-Amundsen¹ and V. Yu. Ponomarev²

¹*Mathematics Institute, University of Munich, Theresienstrasse 39, 80333 Munich, Germany*

²*Institute of Nuclear Physics, Technical University of Darmstadt, 64289 Darmstadt, Germany*

(Received 10 September 2016; published 8 February 2017)

The distorted-wave Born approximation formalism for the description of the $(e, e'\gamma)$ reaction, in which emitted photons and scattered electrons are simultaneously detected, is outlined. Both the Coulomb and the magnetic scattering are fully taken into account. The influence of electron bremsstrahlung is estimated within the plane-wave Born approximation. Recoil effects are also discussed. The formalism is applied for the low-energy $(e, e'\gamma)^{92}\text{Zr}$ reaction with excitation of the first collective (2_1^+) and mixed-symmetry (2_2^+) states. The corresponding transition charge and current densities are taken from a random-phase approximation (RPA) calculation within the quasiparticle phonon model. It is shown, by this example, in which way the magnetic subshell population of the excited state influences the angular distribution of the decay photon. For these quadrupole excitations the influence of magnetic scattering is only prominent at the backmost scattering angles, where a clear distinction of the photon pattern pertaining to the two states is predicted.

DOI: [10.1103/PhysRevC.95.024310](https://doi.org/10.1103/PhysRevC.95.024310)

I. INTRODUCTION

Nuclear excitation by the scattering of fast electrons is a powerful tool to probe the nuclear structure [1,2] since only the well-known electromagnetic interaction between the projectile and the target is involved. The simultaneous detection of photons which are emitted when the excited nucleus decays into its ground state implies a considerable increase of sensitivity to the nuclear structure effects. Such coincidence measurements also allow one to easily separate low-spin excited states at intermediate energies from the background of high-spin states.

A disadvantage of nuclear excitation by electron impact is the presence of electron bremsstrahlung. A photon resulting from nuclear decay into the ground state is indistinguishable from a bremsstrahlung photon (with the same energy) which is emitted by the electron. Therefore this process has to be added coherently to the coincident nuclear excitation and decay process (henceforth called ExDec). Since the energy resolution of the photon detectors is usually orders of magnitude larger than the level width of the low-lying excited states, a considerable fraction of the observed photons may originate from bremsstrahlung. It is therefore important to investigate the angular dependence of both processes in order to choose an experimental setup where the perturbation by bremsstrahlung is minimized.

A pioneer measurement of the ExDec process involved the scattering of 67 MeV electrons from a ^{12}C nucleus and exciting the 2^+ state at 4.439 MeV [3]. The influence of bremsstrahlung was not considered in the theoretical interpretation of this experiment [4], being in wide angular regions unimportant for light nuclei such as carbon. In the calculation of the ExDec process, the distorted-wave Born approximation (DWBA) was used for the charge contribution, but not for the current contribution to nuclear excitation. The Coulomb distortion was found to have a very small effect on the photon angular distribution.

The first theoretical investigation of the ExDec process, including bremsstrahlung, dates back to Hubbard and Rose [5],

and was subsequently applied to the excitation of ^{12}C and ^{16}O nuclei [6]. Use had been made of the plane-wave Born approximation (PWBA) for the inelastic electron scattering, together with simple models for the nuclear transition densities.

Recently, the excitation of the first collective (2_1^+) and mixed-symmetry (2_2^+) states in ^{92}Zr has been studied in (e, e') and (p, p') reactions [7]. A different q dependence of the (p, p') cross sections and a similar q dependence of the (e, e') cross sections for these two states was established. This fact was ascribed to interference effects between valence-shell and cross-shell excitations in the structure of the two states [7]. An extension of these studies by the $(e, e'\gamma)^{92}\text{Zr}$ reaction is planned [8]. In the present work we consider predictions for this reaction as an example of the ExDec process on medium heavy spin-zero nuclei. The nuclear transition charge and current densities are calculated within the quasiparticle random-phase approximation (QRPA) and the quasiparticle phonon model (QPM) [9]. For the scattering process the DWBA is applied throughout.

For bremsstrahlung an exact relativistic prescription using Dirac partial waves for the electronic scattering states has become standard [10–12], but this theory is no longer feasible at collision energies exceeding 30 MeV [13]. Therefore we use the PWBA [14–16], but provide an estimate of its accuracy by comparing it with the fully relativistic calculations for the same collision geometry at lower impact energies.

The paper is organized as follows. Section II provides the theoretical formalism. For simplicity a spin-zero ($J_{g.s.} = 0$) nucleus is assumed (which covers all even-even nuclei). The formalism can easily be extended to $J_{g.s.} \neq 0$ nuclei as well. Recoil effects are considered in Sec. III and the computational details are supplied in Sec. IV. Results for the first and second 2^+ states of ^{92}Zr are given in Sec. V. The conclusion is drawn in Sec. VI. Atomic units ($\hbar = m = e = 1$) are used unless indicated otherwise.

II. THEORETICAL FORMALISM

Let us consider the collision of a relativistic electron with a spin-zero nucleus at rest. The cross section for the inelastic

scattering of the electron with the simultaneous emission of a photon consists of three contributions, the amplitudes of which have to be added coherently. The dominant contribution to the ExDec process (henceforth denoted by $W_{fi}^{(1)}$) describes the process where in the first step the nucleus is excited from the ground state to a quasistationary state with decay width Γ_n . Subsequently the excited nucleus decays via the emission of a photon. A second, in general much smaller, contribution arises from the reversed process (to be termed $W_{fi}^{(2)}$) where the photon emission precedes the nuclear excitation. The third contribution is electron bremsstrahlung, provided the ExDec photon results from the decay to the nuclear ground state.

A. Excitation followed by decay ($W_{fi}^{(1)}$)

In the two-photon approximation $W_{fi}^{(1)}$ accounts for the coupling of electron and nucleus by a virtual photon and the coupling of the nucleus to a real photon, and hence is a third-order process. It is calculated from [5]

$$\begin{aligned} W_{fi}^{(1)} &= \left(\frac{-ie}{c}\right)^3 Z_T \int d^4x_e \sum_{\nu=0}^3 \sum_{\mu=1}^3 \int d^4x_N d^4y_N \\ &\times \sum_n \langle \phi_f | J_\mu(y_N) | \phi_n \rangle \langle \phi_n | J_\nu(x_N) | \phi_i \rangle \theta(t_{y_N} - t_{x_N}) \\ &\times \langle \psi_f | j^\nu(x_e) | \psi_i \rangle i c D_0(x_e - x_N) A^\mu(k, y_N). \end{aligned} \quad (2.1)$$

In this expression ϕ_i and ϕ_f are the initial and final nuclear states with energy $E_{\text{nuc},i}$ and $E_{\text{nuc},f}$, respectively, while ϕ_n is the intermediate state with a time dependence $e^{-i(E_{\text{nuc},n} - i\Gamma_n/2)t}$. The initial and final scattering states of the electron with total energies E_i and E_f , respectively, are described by ψ_i and ψ_f . Z_T is the nuclear charge number which arises from the coupling to the real photon (whereas an additional factor $-Z_T$ from the electron-nucleus coupling is absorbed into the electronic scattering states), and $\theta(\tau)$ is the Heaviside step function. The nuclear and electronic transition charge and current density operators are denoted by J_ν and j^ν , respectively [17], $x_N = (ct_{x_N}, \mathbf{x}_N)$ and y_N refer to the nuclear coordinates, and x_e is the electronic coordinate. The photon propagator D_0 and the photon field A^μ are given by

$$\begin{aligned} D_0(x_e - x_N) &= -\frac{1}{(2\pi)^4} \int d^4q \frac{e^{-iq(x_e - x_N)}}{q^2 + i\epsilon} \\ &= \frac{1}{8\pi^2} \int dq_0 e^{-iq_0(ct_e - t_{x_N})} \frac{e^{iq_0|\mathbf{x}_e - \mathbf{x}_N|}}{|\mathbf{x}_e - \mathbf{x}_N|}, \\ A^\mu(k, y_N) &= \frac{c}{2\pi\sqrt{\omega}} \epsilon_\lambda^{\mu*} e^{i\omega t_{y_N}} e^{-ik y_N}, \end{aligned} \quad (2.2)$$

where $\omega = kc$ is the photon frequency, \mathbf{k} is the photon momentum, and ϵ_λ describes the photon polarization. After performing all trivial time and energy integrals, $W_{fi}^{(1)}$ can be written as a superposition of terms, each corresponding to a particular intermediate state. These terms are products of the transition amplitude A_{ni}^{exc} for excitation to the state ϕ_n , and of the amplitude A_{fn}^{dec} for the successive decay to the state ϕ_f .

Explicitly, for the ground-state decay ($E_{\text{nuc},f} = E_{\text{nuc},i}$),

$$\begin{aligned} W_{fi}^{(1)} &= i \frac{Z_T c^2}{4\pi\sqrt{\omega}} \delta(E_f - E_i + \omega) \frac{1}{\omega - E_x + i\Gamma_n/2} \\ &\times \sum_{M_n} A_{ni}^{\text{exc}}(M_i, M_n) A_{fn}^{\text{dec}}(M_n, M_f), \end{aligned} \quad (2.3)$$

where for an excited state with fixed spin J_n the sum runs over the corresponding magnetic substates M_n . E_x is the energy of the excited state and $e = 1$ is used.

Given the general case of an initial state with spin J_i and magnetic quantum number M_i , the excitation amplitude is defined by [1]

$$\begin{aligned} A_{ni}^{\text{exc}}(M_i, M_n) &= -\frac{1}{c} \sum_{\nu=0}^3 \int d\mathbf{x}_e d\mathbf{x}_N \langle \phi_n | J_\nu(\mathbf{x}_N) | \phi_i \rangle \\ &\times \langle \psi_f | j^\nu(\mathbf{x}_e) | \psi_i \rangle \frac{1}{|\mathbf{x}_e - \mathbf{x}_N|} e^{\frac{i}{c}|E_f - E_i||\mathbf{x}_e - \mathbf{x}_N|}. \end{aligned} \quad (2.4)$$

For its evaluation, the conventional partial-wave expansions are used for the wave functions of the electron and for the propagator [17,18]. The nuclear transition matrix elements are partial-wave expanded in the following way [2]:

$$\langle \phi_n | J_\nu(\mathbf{x}_N) | \phi_i \rangle = \sqrt{4\pi} \begin{cases} Q_{ni}(\mathbf{x}_N), & \nu = 0, \\ \mathbf{j}_{ni}(\mathbf{x}_N), & \nu = 1, 2, 3, \end{cases} \quad (2.5)$$

with

$$\begin{aligned} Q_{ni}(\mathbf{x}_N) &= \sum_{LM} (J_i M_i L M | J_n M_n) Q_L(\mathbf{x}_N) Y_{LM}^*(\hat{\mathbf{x}}_N), \\ \mathbf{j}_{ni}(\mathbf{x}_N) &= -i \sum_{L'LM} (J_i M_i L M | J_n M_n) J_{L'L}(\mathbf{x}_N) \mathbf{Y}_{L'L}^{M*}(\hat{\mathbf{x}}_N), \end{aligned} \quad (2.6)$$

where here and in the following x denotes the modulus of \mathbf{x} . Y_{LM} and $\mathbf{Y}_{L'L}^M$ are scalar and vector spherical harmonics, respectively, and $(J_i M_i L M | J_n M_n)$ are Clebsch-Gordan coefficients [19]. The nuclear properties are inherent in the nuclear charge (Q_L) and current ($J_{L'L}$) transition densities. Details of the evaluation of A_{ni}^{exc} in the DWBA formalism can be found in Refs. [1,17,20,21].

The decay amplitude to the final state with quantum numbers J_f and M_f is defined by

$$A_{fn}^{\text{dec}}(M_n, M_f) = \int d\mathbf{y}_N \langle \phi_f | \epsilon_\lambda^* \mathbf{J}(\mathbf{y}_N) | \phi_n \rangle e^{-ik y_N}. \quad (2.7)$$

For the decay into the 0^+ ground state, to be considered here, the transition current density $J_{L'L}(y_N)$ is identical to the transition current density for excitation. Also excitation and decay are mediated in this case by one single multipole L . Upon partial-wave expanding the photon field [19],

$$e^{-ik y_N} = 4\pi \sum_{lm} (-i)^l j_l(k y_N) Y_{lm}^*(\hat{\mathbf{k}}) Y_{lm}(\hat{\mathbf{y}}_N), \quad (2.8)$$

where $j_l(x)$ is a spherical Bessel function, the decay amplitude reduces to

$$A_{fn}^{\text{dec}}(M_n, M_f) = -4\pi i (J_n M_n L M | J_f M_f) \sum_{L'} (-i)^{L'} \times \sum_{\mu, \varrho} (\mathbf{e}_\varrho^+ \boldsymbol{\epsilon}_\lambda^*) (L' \mu 1 \varrho | L M) Y_{L'\mu}^*(\hat{\mathbf{k}}) R_{L'}(k). \quad (2.9)$$

The radial integral in Eq. (2.9) is given by

$$R_{L'}(k) = \int_0^\infty r^2 dr j_{L'}(kr) J_{LL'}(r). \quad (2.10)$$

Its calculation is straightforward since $J_{LL'}(r)$ vanishes rapidly outside the nucleus. For a given L , the angular momentum L' is determined by parity and angular momentum conservation ($L' = L \pm 1$ if the parity of the transition is $(-1)^{L'}$, otherwise $L' = L$ [2]). \mathbf{e}_ϱ is a spherical unit vector and M is determined by $M = M_f - M_n$.

B. Reversed process ($W_{fi}^{(2)}$)

If the photon is emitted prior to nuclear excitation, the corresponding transition amplitude $W_{fi}^{(2)}$ reads

$$W_{fi}^{(2)} = \left(\frac{-ie}{c} \right)^3 Z_T \int d^4 x_e \sum_{\nu=0}^3 \sum_{\mu=1}^3 \int d^4 x_N d^4 y_N \times \sum_n \langle \phi_f | J_\nu(x_N) | \phi_n \rangle \langle \phi_n | J_\mu(y_N) | \phi_i \rangle \theta(t_{x_N} - t_{y_N}) \times \langle \psi_f | j^\nu(x_e) | \psi_i \rangle i c D_0(x_e - x_N) A^\mu(k, y_N). \quad (2.11)$$

This can be transformed into the following expression:

$$W_{fi}^{(2)} = -i \frac{Z_T}{2} \frac{c^2}{2\pi\sqrt{\omega}} \delta(E_f - E_i + \omega) \frac{1}{\omega + E_x - i\Gamma_n/2} \times \sum_{M_n} A_{fn}^{\text{exc}}(M_n, M_f) A_{ni}^{\text{dec}}(M_i, M_n). \quad (2.12)$$

It can be shown that, for the spin-0 nuclei, $W_{fi}^{(2)}$ differs from $W_{fi}^{(1)}$ only by the sign and the resonance denominator.

C. Electron bremsstrahlung

It is assumed that the nucleus remains in this process in its ground state throughout the collision. For a $J_{\text{g.s.}} = 0$ nucleus considered in this paper, electron bremsstrahlung results only from the charge interaction between electron and nucleus [14] (the case of $J_{\text{g.s.}} \neq 0$ is treated in Ref. [15]). Then, in the one-photon approximation, the corresponding transition amplitude is given by

$$W_{fi}^{\text{brems}} = -\frac{ie}{c} \sum_{\mu=1}^3 \int d^4 x_e \langle \psi_f | j_\mu(x_e) A^\mu(k, x_e) | \psi_i \rangle = \frac{ic}{\sqrt{\omega}} \delta(E_f - E_i + \omega) \int d\mathbf{x}_e \langle \psi_f | \boldsymbol{\alpha} \boldsymbol{\epsilon}_\lambda^* | \psi_i \rangle e^{-i\mathbf{k}\mathbf{x}_e}, \quad (2.13)$$

where $\boldsymbol{\alpha}$ is a vector of Dirac matrices.

D. Total cross section

In the following we will assume that the polarization degrees of freedom remain unobserved. In order to obtain the total cross section one has therefore to average over the initial ($\boldsymbol{\zeta}_i$ and M_i) and sum over the final spin polarization ($\boldsymbol{\zeta}_f$ and M_f) of the electron and nucleus, respectively, and also to sum over the photon polarization $\boldsymbol{\epsilon}_\lambda$. Therefore, collecting terms and setting $J_i = J_f = 0$ [5],

$$\frac{d^3\sigma_{\text{tot}}}{d\omega d\Omega_k d\Omega_f} = \frac{4\pi^2 \omega^2 E_i E_f k_f}{k_i c^5} \frac{1}{2} \sum_{\zeta_i} \sum_{\zeta_f} \sum_{\lambda} \times \left| \frac{1}{c} M_{fi}^{\text{brems}} + \frac{1}{c} (M_{fi}^{(1)} + M_{fi}^{(2)}) \right|^2, \quad (2.14)$$

where M_{fi} is defined by $W_{fi} = \delta(E_f - E_i + \omega) M_{fi}$ according to the equations (2.3), (2.12), and (2.13). When $\boldsymbol{\zeta}_f$ is chosen along \mathbf{k}_f (the electron momentum in its final state), the cross section is independent of the sign of $\boldsymbol{\zeta}_f$ such that the sum over $\boldsymbol{\zeta}_f$ reduces to a factor of 2.

If there are more decay channels of the excited state, the transition amplitudes $M_{fi}^{(1)}$ and $M_{fi}^{(2)}$ have to be multiplied by the square root of the branching ratio Γ_{n0}/Γ_n , where Γ_{n0} is the partial decay width of ϕ_n to the ground state, while Γ_n is the total decay width of ϕ_n [6].

III. RECOIL EFFECTS

In the formalism of the previous section recoil effects due to the finite mass M_T of the target nucleus have been neglected. Particularly for the lighter nuclei or for very high collision energies this is no longer a good approximation, most importantly because a finite momentum of the nucleus shifts the photon frequency out of resonance [22]. In the following the various contributions to recoil are derived. Thereby, the reference frame is the laboratory frame throughout, where the nucleus is initially at rest.

A. Recoil concerning excitation plus decay

For a given excitation energy ω_{ex} (which may differ from the level energy E_x due to the finite width Γ_n), the energy E_f of the scattered electron is calculated from energy-momentum conservation,

$$E_i + E_{\text{nuc},i} = E_f + E_{\text{nuc},n} \\ \mathbf{k}_i = \mathbf{k}_f + \mathbf{q}_n, \quad (3.1)$$

where $E_{\text{nuc},i} = M_T c^2$ and $E_{\text{nuc},n} = \sqrt{q_n^2 c^2 + M_T^2 c^4} + \omega_{\text{ex}}$. The result for E_f is lengthy and is given, e.g., in Ref. [20]. In particular, it depends on the electron scattering angle ϑ_f and is slightly lower than $E_i - \omega_{\text{ex}}$ (the value attained for $M_T \rightarrow \infty$).

After excitation the nucleus decays to the ground state, emitting a photon of frequency ω . This frequency is again derived from the conservation of energy and momentum,

$$E_{\text{nuc},n} = E_{\text{nuc},f} + \omega \\ \mathbf{q}_n = \mathbf{q}_f + \mathbf{k}, \quad (3.2)$$

where $E_{\text{nuc},f} = \sqrt{q_f^2 c^2 + M_T^2 c^4}$ and, with (3.1), $\mathbf{q}_f = \mathbf{k}_i - \mathbf{k}_f - \mathbf{k}$. Upon squaring $E_{\text{nuc},f}$ from (3.2) one obtains

$$\begin{aligned} \omega &= kc \\ &= \frac{1}{2} \frac{\omega_{ex}^2 + 2\omega_{ex} \sqrt{q_n^2 c^2 + M_T^2 c^4}}{\omega_{ex} + \sqrt{q_n^2 c^2 + M_T^2 c^4} - k_i c \cos \theta_k + \hat{\mathbf{k}} \mathbf{k}_f c}, \end{aligned} \quad (3.3)$$

where θ_k is the photon emission angle and $\mathbf{q}_n = \mathbf{k}_i - \mathbf{k}_f$. It is readily seen that for $M_T \rightarrow \infty$, $\omega \rightarrow \omega_{ex}$, but otherwise ω can be above or below ω_{ex} , depending on the directions $\hat{\mathbf{k}}$ and $\hat{\mathbf{k}}_f$ of photon and scattered electron, respectively.

Apart from affecting the energy of the outgoing particles, recoil also modifies the cross section in terms of a recoil factor f_{rec}^{-1} [2] which arises from the integration of the transition probability over E_f with the help of the energy-conserving δ -function, $\delta(E_i + E_{\text{nuc},i} - E_f - E_{\text{nuc},f} - \omega)$. It is given by [16]

$$f_{\text{rec}} = 1 - \frac{\mathbf{k}_f \mathbf{q}_f E_f}{k_f^2 E_{\text{nuc},f}}. \quad (3.4)$$

Note that the excitation energy ω_{ex} enters into the resonance factors in Eqs. (2.3) and (2.12) by means of $1/(\omega_{ex} - E_x + i\Gamma_n/2)$ and $1/(\omega_{ex} + E_x - i\Gamma_n/2)$, respectively.

B. Recoil in the bremsstrahlung process

For the spin-zero nuclei considered here, only the kinematical recoil has to be considered, whereas the dynamical recoil (bremsstrahlung emission by the nucleus [23]) is absent. For a coherent superposition of nuclear decay and bremsstrahlung it is necessary that, when measuring the photon energy, one cannot distinguish its origin. Accordingly, the bremsstrahlung amplitude W_{fi}^{brems} has to be calculated for the ω determined from (3.3). The energy of the scattered electron is then obtained from energy-momentum conservation for the bremsstrahlung process,

$$\begin{aligned} E_i + E_{\text{nuc},i} &= \tilde{E}_f + \tilde{E}_{\text{nuc},f} + \omega, \\ \mathbf{k}_i &= \tilde{\mathbf{k}}_f + \mathbf{P}_f + \mathbf{k}, \end{aligned} \quad (3.5)$$

with $\tilde{E}_{\text{nuc},f} = \sqrt{P_f^2 c^2 + M_T^2 c^4}$ and $\mathbf{P}_f = \mathbf{k}_i - \tilde{\mathbf{k}}_f - \mathbf{k}$. The respective formula for \tilde{E}_f can be found in Ref. [16].

From the conservation of the total energy it follows that $E_f + E_{\text{nuc},f} = \tilde{E}_f + \tilde{E}_{\text{nuc},f}$, and one can show by contradiction that, for a fixed direction $\hat{\mathbf{k}}_f = \hat{\mathbf{k}}_f$, $\tilde{\mathbf{k}}_f = k_f$ is the only solution. This implies that if the photons from nuclear decay and bremsstrahlung are indistinguishable in the photon detector, so are the electrons from the respective processes in the electron detector. Hence nuclear decay and bremsstrahlung are always coherently contributing, irrespective of the detector resolutions.

IV. COMPUTATIONAL DETAILS

A. Nuclear structure part

The transition charge and current densities have been calculated within the quasiparticle-phonon model (QPM) [9]. Details of their calculation can be found in Ref. [21]. We recall

only their formal expression in QRPA for an excitation of the i th one-phonon state,

$$\varrho_{Li}(r) = \sum_{jj'}^{n,p} (u_j v_{j'} + v_j u_{j'}) (X_{jj'}^{Li} + Y_{jj'}^{Li}) \varrho_{jj'}^L(r) \quad (4.1)$$

$$J_{LL'i}(r) = \sum_{jj'}^{n,p} (u_j v_{j'} - v_j u_{j'}) (X_{jj'}^{Li} - Y_{jj'}^{Li}) J_{jj'}^{LL'}(r), \quad (4.2)$$

where u_j and v_j are the coefficients of the Bogoliubov transformation from particles to quasiparticles (their squares are the occupation numbers of the mean-field level $j = |nlj\rangle$ for holes and particles, respectively). X and Y are the phonon's forward and backward amplitudes. The quantities $\varrho_{jj'}^L(r)$ and $J_{jj'}^{LL'}(r)$ in Eqs. (4.1) and (4.2) are the particle-hole charge and current transition densities, respectively.

The charge transition densities $\varrho_L(r)$ of the collective (2_1^+) and mixed-symmetry (2_2^+) states in ^{92}Zr ($L = 2^+$) are given in Fig. 2 of [7]. As discussed in Ref. [7], they can be represented as a superposition of the contributions from the dominant two-quasiparticle valence-shell configurations [$\nu(2d_{5/2})^2$ and $\pi(1g_{9/2})^2$] and of the collective part from the giant quadrupole resonance (GQR). The neutron $\nu(2d_{5/2})^2$ component in the wave function of the 2_2^+ state changes sign as compared to the 2_1^+ state while the sign of the $\pi(1g_{9/2})^2$ component remains unchanged. As a result of the interference between the two-quasiparticle and the collective GQR components, the total proton transition densities of the 2_1^+ and 2_2^+ states look very much alike. At the same time, the total neutron transition density of the 2_1^+ state is peaking at larger radii as compared to the one of the 2_2^+ state. Thus the q dependence of the (e, e') scattering cross section for not too backmost angles [which depends only on the proton $\varrho_L(r)$] is predicted to be the same for both states. The (p, p') cross section depends on both the proton and neutron parts of $\varrho_L(r)$ and accordingly one expects a shift to higher q -values for the 2_2^+ state. These predictions have been experimentally confirmed [7].

The QPM current densities $J_{L,L'}(r)$ of the 2_1^+ and 2_2^+ states in ^{92}Zr are plotted in Fig. 1. They are composed of the convection and magnetization currents. The contribution of the convection current to the total current densities is rather small. Note that the valence-shell two-quasiparticle $\nu(2d_{5/2})^2$ and $\pi(1g_{9/2})^2$ configurations, important for the charge transition densities in this nucleus, give no contribution to the current densities due to the factor $(u_j v_{j'} - v_j u_{j'})$ in Eq. (4.2). Both $J_{21}(r)$ and $J_{23}(r)$ are larger for the 2_2^+ state while the opposite is true for $\varrho_2(r)$. In our calculations the more transparent QRPA prescription for the transition densities is used. In fact, QPM and QRPA provide the same relative M_n -subshell populations in the excitation process, while differing slightly in the absolute cross section.

B. Reaction part

The partial waves used for the electronic scattering states are obtained with the help of the Fortran code RADIAL of Salvat *et al.* [24]. They are solutions to the Dirac equation in the nuclear potential generated from the ground-state charge distribution, which for ^{92}Zr is tabulated in terms of a Fourier-Bessel expansion [25].

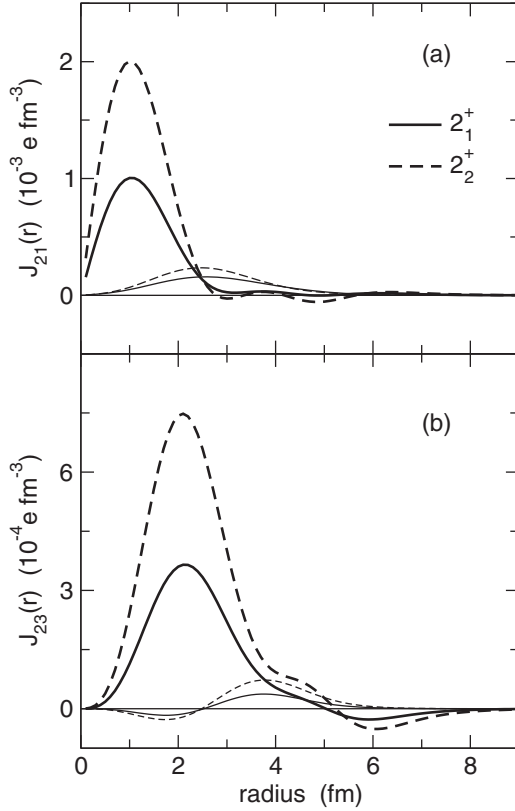


FIG. 1. Current densities $J_{L,L'}(r)$ of the 2_1^+ and 2_2^+ states in ^{92}Zr for $L' = L - 1$ (a) and $L' = L + 1$ (b). Separately shown is the contribution of the convection current (thin lines) to the total current (thick lines).

The total decay widths of the 2_1^+ and 2_2^+ states of ^{92}Zr (at energies $E_x = 0.9345$ MeV and 1.847 MeV, respectively) were determined experimentally to $\Gamma_n = 9.1 \times 10^{-8}$ keV and 4.706×10^{-6} keV, respectively, and the branching ratios Γ_{n0}/Γ_n are unity for the lower and 0.309 for the higher 2^+ state [7,26]. The LaBr photon detector, to be used in the planned experiments [8,27], has a resolution $\Delta\omega$ of 3% of the photon energy ω , amounting to 30-60 keV. Therefore, an average of the cross section over $\Delta\omega$ is mandatory, such that (2.14), including recoil, turns in the peak maximum into

$$\begin{aligned} \left\langle \frac{d^3\sigma_{\text{tot}}(E_x)}{d\omega d\Omega_k d\Omega_f} \right\rangle_{\Delta\omega} &= \frac{1}{\Delta\omega} \frac{4\pi^2\omega^2 E_i E_f k_f}{k_i c^5} \frac{1}{f_{\text{rec}}} \frac{1}{2} \\ &\times \sum_{\xi_i} \sum_{\xi_f, \lambda} \int_{E_x - \Delta\omega/2}^{E_x + \Delta\omega/2} d\omega_{ex} \left| \frac{1}{c} M_{fi}^{\text{brems}} \right. \\ &\left. + \frac{1}{c} \sqrt{\frac{\Gamma_{n0}}{\Gamma_n}} M_{fi}^{(1)} \right|^2. \end{aligned} \quad (4.3)$$

We have dropped the contribution $M_{fi}^{(2)}$ from the reversed process, as it is, at any excitation energy, orders of magnitude below the sum of $M_{fi}^{(1)}$ and M_{fi}^{brems} .

The shape of the integrand is basically determined by the resonance factor from $M_{fi}^{(1)}$ in Eq. (2.3). Taking into

consideration that the variation of M_{fi}^{brems} and of $(\omega_{ex} - E_x + i\Gamma_n/2)M_{fi}^{(1)}$ is small, both quantities can be approximated by their values for $\omega_{ex} = E_x$, if ω_{ex} changes by some tens of keV. This speeds up the integration procedure considerably. Note that (4.3) is not valid in the wings of the peak where detector statistics lead to a Gaussian peak shape [3,8].

For the evaluation of the transition amplitudes a coordinate system is chosen which is the same as for nuclear excitation. The z axis is taken along the direction \hat{k}_i of the incident electron, the y axis along $\hat{k}_i \times \hat{k}_f$ and the x axis along $\mathbf{e}_y \times \hat{k}_i$, such that \mathbf{k}_f lies in the (x, z) plane (which is called scattering plane). Therefore, the photon momentum \mathbf{k} is given by $\mathbf{k} = D_z \mathbf{k}_0$ where $\mathbf{k}_0 = k(\sin\theta_k, 0, \cos\theta_k)$ lies in the (x, z) plane and D_z is a rotation matrix,

$$D_z = \begin{pmatrix} \cos\varphi & -\sin\varphi & 0 \\ \sin\varphi & \cos\varphi & 0 \\ 0 & 0 & 1 \end{pmatrix}, \quad (4.4)$$

which rotates \mathbf{k}_0 out of the scattering plane by the azimuthal angle φ to give the general representation of \mathbf{k} in spherical coordinates. Correspondingly, the conventional basis vectors for the linear photon polarization must also be rotated,

$$\begin{aligned} \epsilon_{\lambda_1} &= D_z \begin{pmatrix} 0 \\ 1 \\ 0 \end{pmatrix} = \begin{pmatrix} -\sin\varphi \\ \cos\varphi \\ 0 \end{pmatrix}, \\ \epsilon_{\lambda_2} &= D_z \begin{pmatrix} -\cos\theta_k \\ 0 \\ \sin\theta_k \end{pmatrix} = \begin{pmatrix} -\cos\theta_k \cos\varphi \\ -\cos\theta_k \sin\varphi \\ \sin\theta_k \end{pmatrix}. \end{aligned} \quad (4.5)$$

It is convenient to represent the polarization vectors in terms of the spherical unit vectors, $\epsilon_{\lambda}^* = \sum_{\mu} c_{\mu}^{(\lambda)} \mathbf{e}_{\mu}$. For λ_1 and λ_2 , the coefficients are

$$\begin{aligned} c_0^{(1)} &= 0, \quad c_{+1}^{(1)} = \frac{i}{\sqrt{2}} e^{-i\varphi}, \quad c_{-1}^{(1)} = \frac{i}{\sqrt{2}} e^{i\varphi}, \\ c_0^{(2)} &= \sin\theta_k, \quad c_{+1}^{(2)} = \frac{\cos\theta_k}{\sqrt{2}} e^{-i\varphi}, \quad c_{-1}^{(2)} = -\frac{\cos\theta_k}{\sqrt{2}} e^{i\varphi}. \end{aligned} \quad (4.6)$$

With this representation it follows that in Eq. (2.9), $\mathbf{e}_{\lambda}^+ \epsilon_{\lambda}^* = c_{\lambda}^{(\lambda)}$.

The bremsstrahlung amplitude is calculated within the PWBA, including form factors, as described in Ref. [16]. Figure 2 shows the comparison between the PWBA and the Dirac partial-wave (DW) theory [13] for the emission of a photon with $\omega = 1.847$ MeV in 10 MeV $^{92}\text{Zr}(e, e')$ collisions at a scattering angle $\vartheta_f = 40^\circ$. The energy of 10 MeV was chosen because of convergence problems for higher energies at the larger angles. It is seen that the PWBA underestimates the bremsstrahlung cross section by about a factor of 1.3 at all angles. The energy dependence of this Dirac-wave enhancement factor is very weak above 10 MeV [13].

Recoil effects increase with scattering angle and with collision energy. For the largest angle ($\vartheta_f = 179^\circ$) we have found that the omission of recoil leads at most to a 2-3% increase of the ExDec cross section throughout the photon angular distribution for collision energies up to 100 MeV.

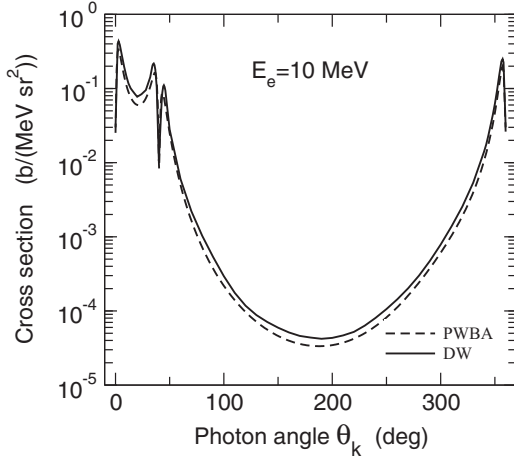


FIG. 2. Triply differential cross section $d^3\sigma/d\omega d\Omega_k d\Omega_f$ for bremsstrahlung emitted in collisions of 10 MeV electrons with ^{92}Zr ($Z_T = 40$) as a function of θ_k . The photon frequency is $\omega = 1.847$ MeV (the 2_2^+ excitation energy), the scattering angle is $\vartheta_f = 40^\circ$, and the azimuthal angle between photon and electron is $\varphi = 0$.

This is about twice as much as the change of the excitation cross section by recoil effects (for the 2^+ states in ^{92}Zr under consideration). Also the kinematical recoil in bremsstrahlung is small for our cases of interest ($\lesssim 1\%$). In our results, recoil is included throughout.

V. RESULTS FOR THE ^{92}Zr NUCLEUS

In this section we will focus on the excitation of the lowest two 2^+ states of ^{92}Zr and on the resulting distribution of the M_n subshells. In the sequel we provide results for the total ExDec process, both with and without the inclusion of bremsstrahlung.

A. Nuclear excitation by electron impact

In Fig. 3(a) the excitation cross sections of the second 2^+ state for a given subshell $M_n = 0, \pm 1, \pm 2$ are displayed at a collision energy of 75 MeV. These cross sections are normalized to the total cross section $d\sigma_{\text{tot}}/d\Omega_f$ (which is an incoherent sum over all subshell contributions [20]). At scattering angles between 30° – 50° all subshells are occupied with similar probability. In particular the sign of M_n does not play much role for the smaller angles. However, at the backward angles the $M_n = 0$ subshell becomes dominant, and close to 180° , where magnetic scattering comes into play, nearly all excitation strength is focused in $M_n = 1$.

The relative M_n -subshell contributions are similar for the excitation to the 2_1^+ state [Fig. 3(b)], except at the backward angles where the $M_n = 1$ contribution for 2_2^+ dominates because of the larger transition current densities. Figure 3(b) also displays the dependence of the $M_n = 0$ and $M_n = 1$ contributions on the collision energy. An increase from 75 to 100 MeV has hardly any effect in the forward hemisphere. However, at large scattering angles there is a strong depletion of $M_n = 0$ in favor of $M_n = 1$ which carries the information on the magnetic transition current densities (the effect of which is

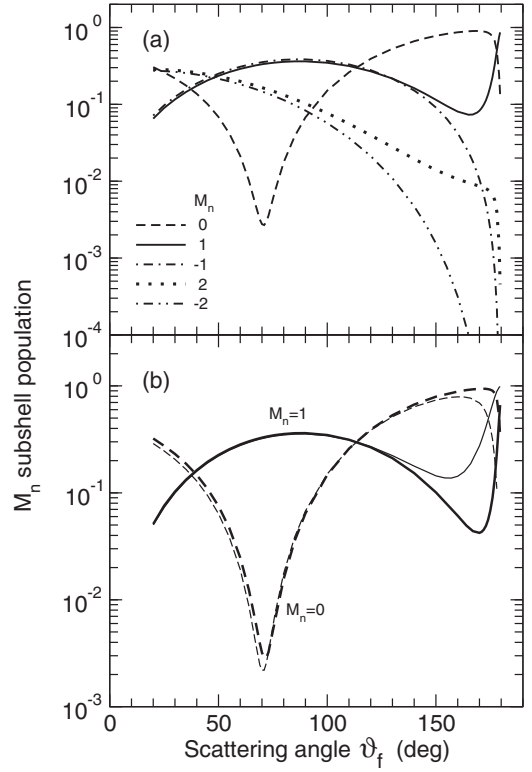


FIG. 3. Relative contribution $\frac{d\sigma_{M_n}}{d\Omega_f} / \frac{d\sigma_{\text{tot}}}{d\Omega_f}$ of a given M_n subshell for the 2^+ state excitation in the $^{92}\text{Zr}(e, e')$ reaction as a function of ϑ_f : (a) 2_2^+ state for a collision energy of 75 MeV; (b) 2_1^+ state for collision energies of 75 MeV (thick lines) and 100 MeV (thin lines).

growing with collision energy). Note that the total excitation cross section decreases with angle and above 60° also with energy when $E_e = E_i - c^2$ is increased from 75 to 100 MeV.

B. Excitation followed by decay

Now we consider the ExDec results. In this subsection we only take into account the contribution from $M_{fi}^{(1)}$ in Eq. (2.14). Since the resonance denominator $(\omega_{ex} - E_x + i\Gamma_n/2)^{-1}$ factors out in this case, the averaging procedure according to (4.3) changes the cross section only by a scaling factor, whereas the shape of the angular or energy distributions remain unaffected. Therefore we also perform no averaging in this subsection. The results are obtained at the excitation energy of the peak maximum, $\omega_{ex} = E_x$.

Figure 4 displays the separate M_n -subshell contributions to the ExDec cross section, which are obtained by retaining only a single M_n state in the sum given in Eq. (2.3), as a function of the photon emission angle θ_k at $\omega_{ex} = 1.847$ MeV. Since only one M_n contributes, each subshell cross section is symmetric with respect to $\theta_k = 180^\circ$ (i.e., it is independent of the azimuthal angle φ). In particular one can show that

$$\begin{aligned} d^3\sigma(M_n = 0)/d\omega d\Omega_k d\Omega_f &\sim B_0 \sin^2 2\theta_k, \\ d^3\sigma(M_n = \pm 1)/d\omega d\Omega_k d\Omega_f &\sim A_{\pm 1} \cos^2 \theta_k + B_{\pm 1} \cos^2 2\theta_k, \\ d^3\sigma(M_n = \pm 2)/d\omega d\Omega_k d\Omega_f &\sim A_{\pm 2} \sin^2 \theta + B_{\pm 2} \sin^2 2\theta. \end{aligned} \quad (5.1)$$

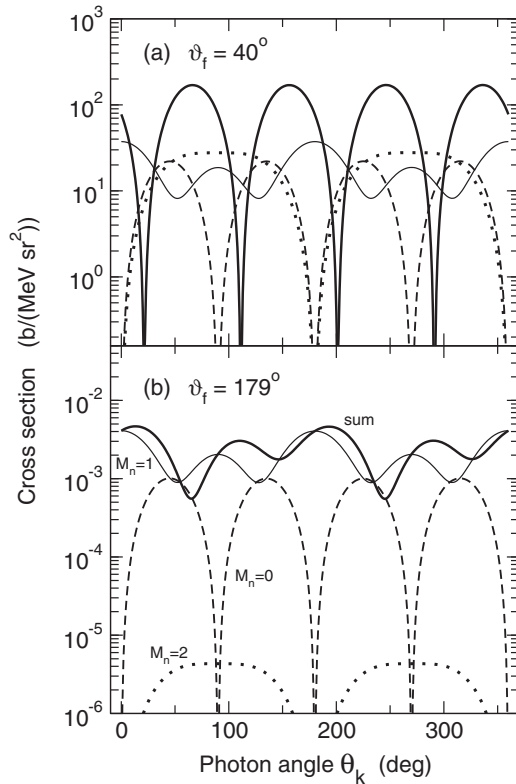


FIG. 4. Triply differential cross section $d^3\sigma/d\omega d\Omega_k d\Omega_f$ for the excitation of the 2_2^+ state of ^{92}Zr by 75 MeV electrons and subsequent photon decay as a function of θ_k : (a) at $\vartheta_f = 40^\circ$, (b) at $\vartheta_f = 179^\circ$, with $\varphi = 0$. Shown are subshell contributions as well as the total cross section from the coherent sum over M_n .

Thereby the quadrupole part of the angular distribution (with coefficients B_n) originates from the contribution of the photon polarization vector ϵ_{λ_2} , whereas the dipole part (with coefficients A_n , being zero for $M_n = 0$) is due to ϵ_{λ_1} (see also Fig. 5). For the $M_n = \pm 2$ states the coefficients $B_{\pm 2}$ are quite small, which results in a dipole-type pattern.

At a scattering angle of 40° [Fig. 4(a)] all subshells contribute with similar weight to the total cross section, and a sign reversal of M_n hardly changes the results [which reflects the behavior of the excitation cross sections; see Fig. 3(a)]. At the backmost angles [Fig. 4(b)] the regular quadrupole pattern of the total cross section, occurring for $\vartheta_f \lesssim 170^\circ$, is modulated by the dominance of the $M_n = 1$ subshell contribution, whereas the $M_n = -1$ and $M_n = \pm 2$ subshells are completely negligible.

The contributions of the two photon polarization directions to the total cross section are illustrated in Fig. 5. Here it is clearly seen that the part resulting from ϵ_{λ_1} (a vector perpendicular to the reaction plane defined by \mathbf{k}_i and \mathbf{k}) gains importance with increasing scattering angle and severely influences the photon angular distribution at the backmost scattering angles.

It is well known from the early studies of the coincident excitation and decay theory [4] that for not too large scattering angles where only the interaction between the charges of electron and nucleus plays a role, the PWBA leads to a

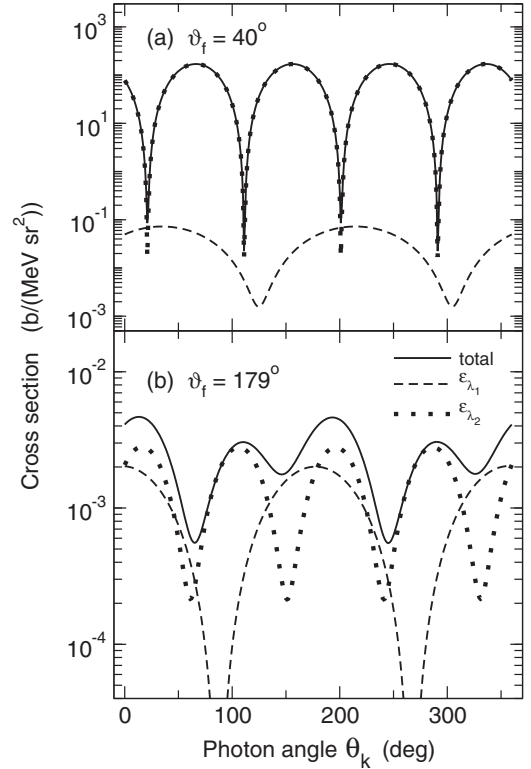


FIG. 5. Triply differential cross section $d^3\sigma/d\omega d\Omega_k d\Omega_f$ for the 2_2^+ excitation and decay of ^{92}Zr by 75 MeV electrons as a function of θ_k at $\varphi = 0$. Shown are the contributions from ϵ_{λ_1} and ϵ_{λ_2} to the total cross section at $\vartheta_f = 40^\circ$ (a) and 179° (b).

photon angular distribution which is azimuthally symmetric with respect to the direction of the momentum transfer $\mathbf{q}_n = \mathbf{k}_i - \mathbf{k}_f$. The shift of the cross section minima obtained from an accurate calculation as compared to the PWBA is therefore a measure of two effects. One is the Coulomb distortion, implemented in the DWBA prescription of electron scattering, which comes into play for the heavier nuclei. However, more important for nuclear structure investigations, a shift is also caused by the presence of the magnetic interaction between the currents of the colliding particles. The previous experimental investigations on the quadrupole excitation of the ^{12}C nucleus at scattering angles in the forward hemisphere ($\vartheta_f = 60^\circ$ and 80° [3]) identified a shift of about 2° , from which the relative sign between the charge and the current contributions to the cross section could be determined. For ^{92}Zr the magnetic interaction is considerably weaker such that the cross section in the forward hemisphere arises only from Coulomb scattering. The resulting shift, due to Coulomb distortion, is about 0.1° for angles below 120° . From Fig. 6 it follows, however, that the shift becomes particularly prominent at the backmost angles, say, above $\vartheta_f = 160^\circ$. Moreover, it is considerably larger for the 2_2^+ excitation (as compared to the 2_1^+ excitation), which shows that its origin is indeed the presence of the magnetic interaction.

Figure 7 compares DWBA and PWBA for the 2_2^+ state at the complete photon angular distribution for the two scattering angles $\vartheta_f = 40^\circ$ and 179° . At 40° the tiny shift between

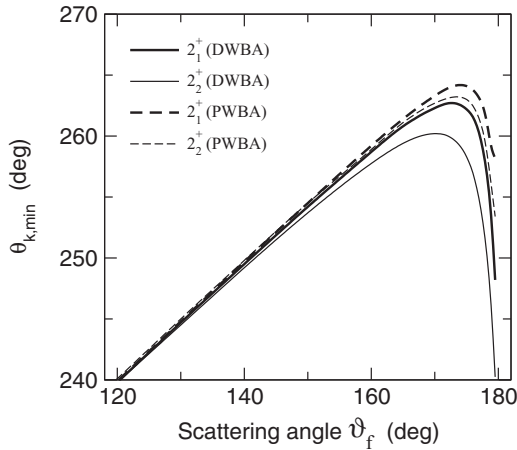


FIG. 6. Location $\theta_{k,\min}$ of one of the minima in the photon angular distribution as a function of ϑ_f from 75 MeV $(e, e'\gamma)^{92}\text{Zr}$ reactions. Shown are the results for 2_1^+ and 2_2^+ excitation within DWBA and PWBA. The PWBA results are obtained by setting $Z_T = 0.01$ in the nuclear potential which generates the electronic scattering states.

the minima from DWBA and PWBA is hardly perceptible; however, the cross section within DWBA is globally enhanced by a factor of 1.5. This situation remains unchanged up to a scattering angle of about 150° . The photon patterns for the 2_1^+

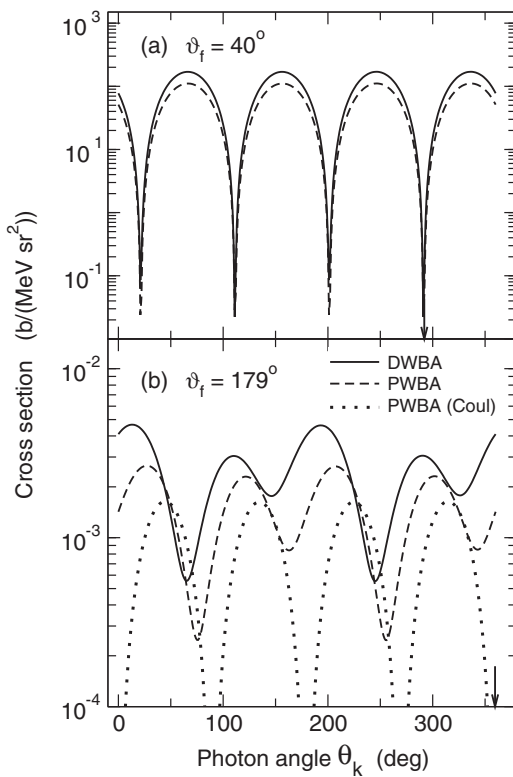


FIG. 7. Triply differential cross section $d^3\sigma/d\omega d\Omega_k d\Omega_f$ for the 2_2^+ excitation in 75 MeV $(e, e'\gamma)^{92}\text{Zr}$ reactions as a function of θ_k at $\vartheta_f = 40^\circ$ (a) and 179° (b) for $\varphi = 0$ within DWBA, PWBA, and the Coulomb contribution to PWBA. In (a), the arrow marks the angle $\theta_q = \angle(\hat{k}_i, \hat{q}_n) = 291.96^\circ$. In (b), the arrow marks $\theta_q = 359.51^\circ$.

and the 2_2^+ states are the same in the forward hemisphere (with the same DWBA enhancement factor); however, the cross section for the 2_1^+ state is about three orders of magnitude larger. At 179° [Fig. 7(b)] where the shift is very large, the influence of magnetic scattering is elucidated within the PWBA by switching off the contribution from the transition current densities. This leads to a shift of the minima by as much as 15° . A further shift (by about 10° for the deeper minimum) is induced by the change from PWBA to DWBA. (For the 2_1^+ state, the shifts are 10° and 6° , respectively.) While the Coulomb-distortion induced shift is small both for Coulomb scattering and magnetic scattering (if considered separately), Coulomb distortion strongly affects the absolute cross sections. Explicitly, at 179° , the Coulomb part of the 2_2^+ state is lowered by a factor of 0.65, whereas the magnetic part is increased by a factor of 2.5. This was not taken into account in the earlier calculations where the magnetic scattering was only treated in PWBA [4]. For the 2_1^+ state where at 179° the magnetic scattering is less important, the Coulomb distortion even leads to a reduction of the total cross section (by a factor of 0.85).

To consider how the interplay between the Coulomb and magnetic contributions influences the photon angular distribution comparison is made between the shape of the angular distributions relating to the 2_1^+ and the 2_2^+ state by normalizing them to equal maximum height (Fig. 8). For a

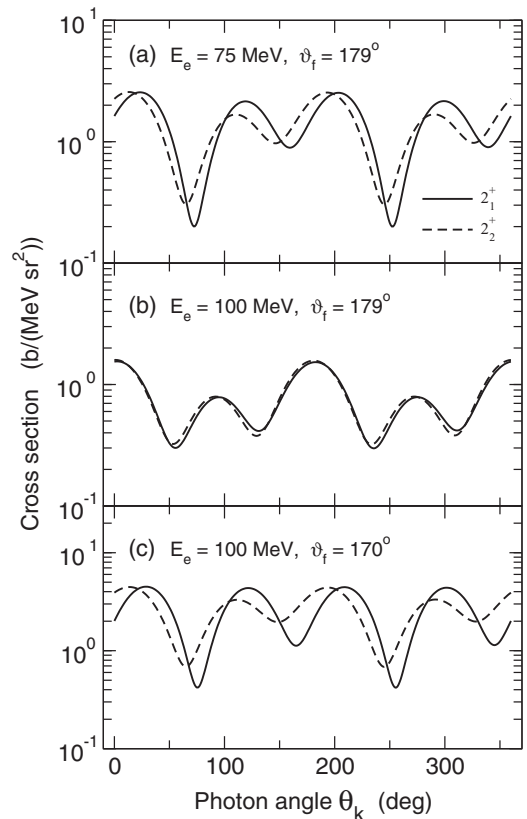


FIG. 8. Triply differential cross section $d^3\sigma/d\omega d\Omega_k d\Omega_f$ from the $(e, e'\gamma)^{92}\text{Zr}$ reaction at $\varphi = 0$ as a function of θ_k . Shown are results for the 2_1^+ and 2_2^+ excitation (the latter multiplied in the graph by a factor F_m). (a) $F_m = 550$, (b) $F_m = 250$, (c) $F_m = 550$.

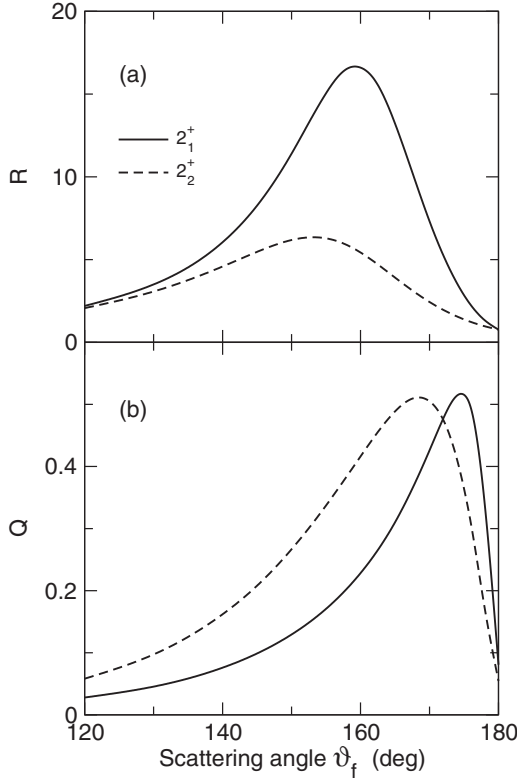


FIG. 9. (a) Cross section ratio $R = \frac{d^3\sigma}{d\omega d\Omega_k d\Omega_f}(\theta_k = 110^\circ) / \frac{d^3\sigma}{d\omega d\Omega_k d\Omega_f}(\theta_k = 80^\circ)$ for the 2_1^+ and 2_2^+ excitation in 100 MeV $(e, e'\gamma)^{92}\text{Zr}$ reactions as a function of ϑ_f at $\varphi = 0$. (b) Ratio Q as a measure of the relative importance of Coulomb and magnetic scattering in 100 MeV $(e, e')^{92}\text{Zr}$ excitation.

collision energy of 75 MeV no difference is seen at 40° . However, at 179° where both Coulomb and magnetic scattering contribute to the cross section (in a different way for the two 2^+ states), the respective cross sections are shifted and of different magnitude in the second maximum [Fig. 8(a)]. In contrast, when the collision energy is increased to 100 MeV, Coulomb scattering is at 179° completely unimportant for both 2^+ states. This leads to a very similar shape of the angular distribution, with a shift of only 2° [Fig. 8(b)]. However, a reduction of the scattering angle to 170° at this energy leads again to a pronounced distinction of the photon patterns pertaining to the two excited states [Fig. 8(c)].

In order to access the different behavior of the 2_1^+ and 2_2^+ states in an experiment it is suggested to measure the cross section at two distinct photon angles θ_{k1} and θ_{k2} and form their ratio R [8]. Such a ratio technique had already been applied in Ref. [3]. In Fig. 9(a) R is plotted as a function of scattering angle for 100 MeV electrons. It is seen that the largest difference between the collective and the mixed-symmetry states occurs in the region $\vartheta_f = 150^\circ$ – 170° . On the other hand, a measure of the relative importance of Coulomb and magnetic scattering in the excitation process is the ratio

$$Q = \sqrt{\frac{d\sigma_{\text{coul}}}{d\Omega_f} \frac{d\sigma_{\text{mag}}}{d\Omega_f}} / \frac{d\sigma_{\text{tot}}}{d\Omega_f}, \quad (5.2)$$

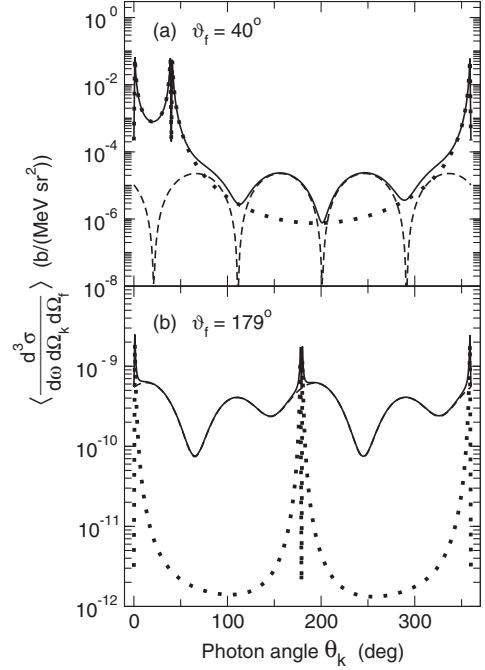


FIG. 10. Cross section averaged over the detector resolution $\Delta\omega/\omega = 3\%$ for the 2_2^+ excitation in 75 MeV $(e, e'\gamma)^{92}\text{Zr}$ reactions at $\vartheta_f = 40^\circ$ (a) and 179° (b) for $\varphi = 0$ as a function of θ_k . Shown are results for the total cross section from (4.3) (solid lines), and for the case where the bremsstrahlung is switched off (dashed lines). The bremsstrahlung background (dotted lines) is shown separately.

where $d\sigma_{\text{coul}}/d\Omega_f$ is the cross section induced by Q_L and $d\sigma_{\text{mag}}/d\Omega_f$ the one resulting from $J_{L, L\pm 1}$ (while $d\sigma_{\text{tot}}/d\Omega_f$ accounts for all three transition densities). When both quantities are equally important, $Q \approx 0.5$ (not precisely 0.5 due to coherence effects). Figure 9(b) supports the conjecture that the maximum deviation between the 2_1^+ and the 2_2^+ states relates to the fact that Coulomb and magnetic scattering contribute nearly equally to the ExDec cross section.

C. Influence of bremsstrahlung

While the cross section for bremsstrahlung is a slowly varying function of the photon frequency which hardly differs when ω is changed within the detector resolution $\Delta\omega$, the averaged ExDec cross section is inversely proportional to $\Delta\omega$ [see (4.3) with M_{fi}^{brems} removed]. Therefore the importance of the bremsstrahlung background to the ExDec process depends strongly on $\Delta\omega$. Using that $\Delta\omega$ is proportional to ω , the bremsstrahlung background is larger for the 2_2^+ excitation. As known from Fig. 2, bremsstrahlung is strongly double-peaked near $\theta_k = 0^\circ$ and $\theta_k = \vartheta_f$. These double-peak structures are clearly visible in the total cross section (4.3) which results from the coherent superposition of the ExDec and the bremsstrahlung transition amplitudes [see Fig. 10(a) for $\vartheta_f = 40^\circ$ where the cross section in the peak maximum is displayed and where $\Delta\omega = 0.03\omega = 55.4$ keV is used for the 2_2^+ decay photon). There is only a small angular region around $\theta_k = 150^\circ$ and 250° where the influence of bremsstrahlung is reduced below 10%, and it is clearly of advantage to place

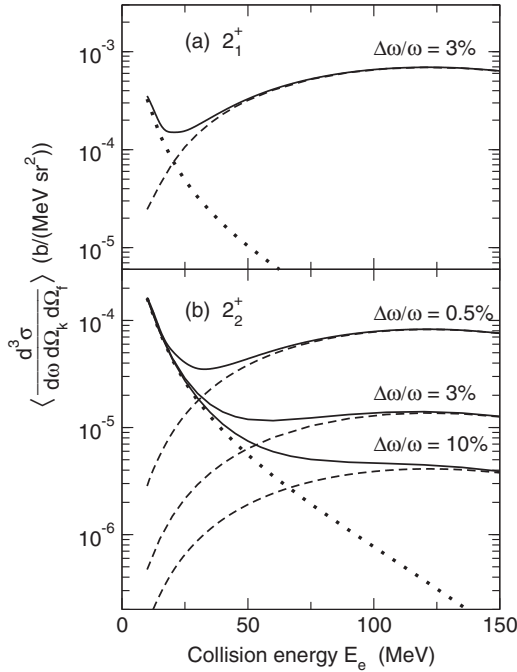


FIG. 11. Cross section averaged over the detector resolution $\Delta\omega/\omega$ for $(e, e'\gamma)^{92}\text{Zr}$ reactions as a function of E_e at $\vartheta_f = 40^\circ$ and $\theta_k = 270^\circ = -90^\circ$ (at $\varphi = 0$ in the peak maximum) with excitation of (a) 2_1^+ and (b) 2_2^+ states. Shown are the ExDec results including bremsstrahlung (solid lines) and without bremsstrahlung (dashed lines). The respective bremsstrahlung results are also shown (dotted lines).

electron and photon detectors in opposite half-planes with respect to the beam axis. The situation improves, however, when the scattering angle gets larger because bremsstrahlung decreases strongly with ϑ_f whereas the increasing magnetic scattering enhances the ExDec cross section. At the backmost angles [see Fig. 10(b) for $\vartheta_f = 179^\circ$] bremsstrahlung plays only a role in the vicinity of the double-peak structures (here near 0° and 180°), which can easily be avoided in the experiment.

Bremsstrahlung becomes less important not only when the scattering angle increases, but also when the electrons are more energetic. This is displayed in Fig. 11 where the averaged cross section with and without the inclusion of bremsstrahlung is plotted as a function of energy. For a scattering angle of 40° and a photon emission angle of 270° (as suggested by the experimentalists) the influence of bremsstrahlung becomes negligible near 50 MeV for the 2_1^+ excitation, but for the 2_2^+ excitation it plays a role up to 100 MeV for the energy resolution $\Delta\omega/\omega = 3\%$.

In Fig. 11(b) it is shown for the 2_2^+ state how the bremsstrahlung background can be suppressed when a detector with a better resolution is used. An improvement from 3% to 0.5% enhances the ExDec cross section by a factor of 6. Thus, for the same geometry, bremsstrahlung can be disregarded above 70 MeV. In contrast, for a poorer resolution of 10%, bremsstrahlung has to be considered up to 150 MeV.

VI. CONCLUSION

In this paper we have considered possible applications of the $(e, e'\gamma)$ reaction to nuclear structure studies. Low-lying quadrupole excitations of ^{92}Zr have been taken as an object. We have shown that for scattering angles ϑ_f of electrons in the forward hemisphere all M_n subshells of the 2^+ states are excited with a similar intensity which results in a regular quadrupole pattern of the photon angular distribution. In contrast, at the backmost scattering angles only the $M_n = 0$ and $M_n = 1$ subshells play a role which leads to an irregular angular distribution. This pattern is composed of a dipole angular distribution resulting from photons polarized perpendicular to the reaction plane, and a shifted quadrupole pattern which is caused by the photons polarized in the reaction plane.

The nuclear structure effects can be visualized by the interplay between the Coulomb and the magnetic scattering. For example, they are supposed to lead to differences in the ExDec process of the two lowest quadrupole states in ^{92}Zr . Unfortunately these effects are not perceptible at forward scattering angles where the predicted cross sections are large. To investigate them, scattering angles around 178° – 180° are required for 75 MeV electrons, where the cross sections have decreased by four orders of magnitude as compared to those near $\vartheta_f = 40^\circ$.

Treating Coulomb and magnetic scattering separately, we have found that at backward angles the effect of Coulomb distortion (i.e., the difference between PWBA and DWBA) leads to a considerable change in the absolute cross section rather than to a shift in the photon angular pattern. However, in the photon angular distribution of the total cross section the shift of the minimum with respect to the azimuthal symmetry axis in PWBA is very large at such backward angles (of the order of 20°). This may lead to a pronounced difference in the angular pattern of the two quadrupole states, depending strongly on collision energy and scattering angle.

We have also estimated how bremsstrahlung, emitted by the electron while the nucleus remains in its ground state, spoils the spectra. The effect depends strongly on the resolution of the photon detector. We conclude that for LaBr detectors bremsstrahlung is of minor importance for the 2_1^+ state. However, for the 2_2^+ state, implying a larger detector resolution, the bremsstrahlung background is high for scattering angles in the forward hemisphere and is only negligible at much higher collision energies (about 100 MeV) or at the backward scattering angles.

To conclude, the $(e, e'\gamma)$ reaction is a challenging test for nuclear models. It provides physical observables which allow to probe nuclear current distributions in excited states of nuclei. The best conditions for that are when the Coulomb and magnetic contributions are equally important.

ACKNOWLEDGMENTS

We thank Profs. N. Pietralla and J. Wambach for encouraging discussions. V.Yu.P. acknowledges support by the DFG (Contracts No. SFB 1245).

- [1] H. Überall, *Electron Scattering from Complex Nuclei* (Academic Press, New York, 1971).
- [2] J. Heisenberg and H. P. Blok, *Annu. Rev. Nucl. Part. Sci.* **33**, 569 (1983).
- [3] C. N. Papanicolas *et al.*, *Phys. Rev. Lett.* **54**, 26 (1985).
- [4] D. G. Ravenhall, R. L. Schult, J. Wambach, C. N. Papanicolas, and S. E. Williamson, *Ann. Phys. (NY)* **178**, 187 (1987).
- [5] D. F. Hubbard and M. E. Rose, *Nucl. Phys.* **84**, 337 (1966).
- [6] H. L. Acker and M. E. Rose, *Ann. Phys. (NY)* **44**, 336 (1967).
- [7] C. Walz, H. Fujita, A. Krugmann, P. von Neumann-Cosel, N. Pietralla, V. Yu. Ponomarev, A. Scheikh-Obeid, and J. Wambach, *Phys. Rev. Lett.* **106**, 062501 (2011).
- [8] N. Pietralla (private communication).
- [9] V. G. Soloviev, *Theory of Atomic Nuclei: Quasiparticles and Phonons* (Institute of Physics, Bristol, 1992).
- [10] H. K. Tseng and R. H. Pratt, *Phys. Rev. A* **3**, 100 (1971).
- [11] H. K. Tseng, *J. Phys. B* **35**, 1129 (2002).
- [12] V. A. Yerokhin and A. Surzhykov, *Phys. Rev. A* **82**, 062702 (2010).
- [13] D. H. Jakubassa-Amundsen, *Phys. Rev. A* **93**, 052716 (2016).
- [14] H. Bethe and W. Heitler, *Proc. R. Soc. London A* **146**, 83 (1934).
- [15] R. A. Berg and C. N. Lindner, *Phys. Rev.* **112**, 2072 (1958).
- [16] D. H. Jakubassa-Amundsen, *Phys. Rev. C* **87**, 064609 (2013).
- [17] S. T. Tuan, L. E. Wright, and D. S. Onley, *Nucl. Instrum. Methods* **60**, 70 (1968).
- [18] E. M. Rose, *Relativistic Electron Theory* (Wiley, New York, 1961), Secs. 15 and 19.
- [19] A. R. Edmonds, *Angular Momentum in Quantum Mechanics*, 2nd ed. (Princeton University Press, Princeton, 1960).
- [20] D. H. Jakubassa-Amundsen, *Nucl. Phys. A* **937**, 65 (2015).
- [21] D. H. Jakubassa-Amundsen and V. Yu. Ponomarev, *Eur. Phys. J. A* **52**, 48 (2016).
- [22] E. Segrè, *Nuclei and Particles* (Benjamin, New York, 1965).
- [23] S. D. Drell, *Phys. Rev.* **87**, 753 (1952).
- [24] F. Salvat, J. M. Fernández-Varea, and W. Williamson Jr., *Comput. Phys. Commun.* **90**, 151 (1995).
- [25] H. De Vries, C. W. De Jager, and C. De Vries, *At. Data Nucl. Data Tables* **36**, 495 (1987).
- [26] C. Fransen *et al.*, *Phys. Rev. C* **71**, 054304 (2005).
- [27] T. Klaus *et al.*, in Proceedings of the DPG Spring Conference, Darmstadt, Germany, HK45.69, 2016, www.dpg-verhandlungen.de/year/2016/conference/darmstadt.